Carrier-based Discontinuous PWM Modulation for Current Source Converters

Olorunfemi Ojo, Sravan Vanaparthy
Department of Electrical and Computer Engineering
Tennessee Electric Machines and Power Electronics Laboratory/Center for Electric Power
Tennessee Technological University, Cookeville, TN 38505, U.S.A.
Phone : (931)-372-3869, Fax : (931)-372-3436, E-mail : jojo@tntech.edu

***Abstract*- Two generalized discontinuous carrier-based pulse-width modulation (GDPWM) methodologies for three-phase current source converters (CSC) are developed based on the classical space vector method and the carrier-based generalized discontinuous modulation scheme for voltage source converters (VSC) . With feasible operation in both the linear and over-modulation regions, they provide the known advantages of the discontinuous carrier-based modulation in voltage source converters – reduced switching loss and reduced effective switching frequency especially in the over-modulation region. These modulation schemes are implemented for a current source inverter from which experimental results are presented to verify concepts and theory.**

***Index Terms*- Current source converters, generalized discontinuous pulse-width modulation, direct digital space vector, triangle intersection method.**

I. INTRODUCTION

Adjustable-speed motor drives and interfacing converters for utility applications traditionally use three-phase voltage source converters modulated by pulse-width modulation schemes to achieve high system response, reduced current and voltage harmonics and unity or leading power factor of operation. The popularity of this topology is due to the simplicity of dc supply obtained from either controlled or uncontrolled rectifiers, stable open loop and minimum-phase dynamic characteristics and its well understood carrier-based and space vector modulation techniques. Unfortunately, voltage source converters require bi-directional input rectifier for regenerative operation. The switching gives rise to relatively high dv/dt transitions on the phase leg output voltages which leads to increased motor losses in drives, voltage surges and unacceptable electromagnetic interference (EMI) effects. The dual of this converter – the current source converter - is known for their simplicity of structure, reliable short circuit protection, four quadrant regenerative operation and nearly sinusoidal current outputs. The low output rate of change of the voltage resulting from the filtering effect of output capacitors and the direct control of currents make it a premium converter in high power applications such as large synchronous motor drives. There is however the disadvantages of the relatively huge input smoothening inductor and its inherent non-minimum phase characteristics which generally degrades its dynamic performance leading to possible open-loop converter instability.

Unlike the voltage source converters where there are well developed and understood carrier-based triangle intersection pulse-width modulation and direct digital space vector modulation schemes, modulation strategies for current converters are relatively less developed and less transparent [1-5]. Utilizing some of the commonalities and dualities of the voltage and current source converters, space vector modulation strategies optimized for voltage source converters are shown to be applicable with minimal modifications to the current source converters. For closed-loop control, space vector algorithms used for current regulated voltage source converters can be slightly modified for the control of voltage regulated current source converters using the concept of duality [6-8]. Current source converters using thyristors with the advantages of ruggedness, lower cost and high power have been realized using a carrier-based triangle intersection PWM modulation scheme. A controlled switching device placed on the dc bus acts as the freewheeling path ensuring active SCR commutation [9-10]. An integrator-based linearizing pulse-width modulator (LPWM) has also been proposed and implemented ensuring linear output AC voltage magnitude to the input DC voltage [11]. It will be shown in the sequel that the modulation signals used to realize LPWM is one of the possibilities obtained from the proposed direct generalized discontinuous carrier-based PWM scheme for the current source converters set forth in this paper.

This paper makes new contributions and gives more clarity to the understanding and development of carrier-based generalized discontinuous triangle intersection and the direct digital pulse programming space vector based modulation methods of the current source converters. The modulation schemes provide the known advantages obtained in the discontinuous carrier-based and space vector PWM modulation schemes for voltage source inverters especially at high and over-modulation regions. In the first proposal given in Section 2 of this paper, the generalized discontinuous PWM strategy for the voltage source inverters is extended for use in the current source converters; which with the variation of a control phase angle and implementation of shorting routines effectively synthesizes the reference three-phase currents. In the direct carrier-based discontinuous triangle intersection PWM scheme based on the classical space vector methodology set forth in Section 3, the expressions for the generalized discontinuous modulation signals are determined which with a unique triangle intersection comparison scheme

generate appropriate PWM pulses for the current synthesis. The proposed modulation schemes are experimentally implemented in Section 4 for a three-phase converter operating in the linear and over-modulation region to validate theory.

II. MODULATION OF CSC USING VSC GDPWM MODULATION SCHEME

Figure 1 below schematically shows a three-phase current source converter (CSC) and a voltage source converter (VSC). In the current source inverter, diodes are connected in series with the switching devices to ensure uni-directional input current flow and a three-phase capacitor arrangement is connected at the output to impress a voltage source on the load. This converter must satisfy both the current and voltage Kirchoff's laws. The Kirchoff's voltage law imposes the constraint that no two or three top (or bottom) switching devices can be turned on at the same time to avoid short-circuiting the output capacitors. Consequently, only a switching device in the top set of devices and another device in the bottom set of devices must be turned on at all times to ensure current continuity. Also, the two switching devices on only one leg can be turned on at the same time in which case the inductor current free-wheels through the switching devices. Concretely expressed, given the switching functions of the devices shown in Figure 1(b) for the current source converters, then :

$$T_{ap} + T_{bp} + T_{cp} = 1,\ T_{ap}T_{bp} = 0,\ T_{ap}T_{cp} = 0,\ T_{bp}T_{cp} = 0$$

$$T_{ap}T_{bp}T_{cp} = 0,\ T_{an}T_{bn}T_{cn} = 0,\ T_{an}T_{bn} = 0,\quad T_{bn}T_{cn} = 0 \qquad (1)$$

$$T_{an} + T_{bn} + T_{cn} = 1,\ T_{an}T_{cn} = 0$$

When a device is turned on, $T_{ij} = 1$ and it is equal to zero, if turned off for i = a,b,c and j = p, n, where p,n denote top and bottom devices; respectively. The truth table showing the acceptable switching possibilities for the CSC are shown in Table I. There are six active states and three null states. Active states impress currents to the load while null states free-wheel the source inductor current through the shorting of the top and bottom devices in a converter leg and decouples the input side from the output without current transfer to the load. For the VSC shown in Figure 1(a), Kirchoff's voltage law imposes the condition that the top and bottom devices on a converter leg cannot be turned on at the same time – they must switch on complementarily. To ensure active control of the load – provide paths for the load currents at all instances - a device on each leg (three switching devices in all) must be turned all the time. These constraints are expressed mathematically as :

$$S_{ap} + S_{an} = 1,\quad S_{bp} + S_{bn} = 1,\ S_{cp} + S_{cn} = 1 \qquad (2)$$

Switching modes of operation satisfying equation (2) are laid out in Table II. There are six active states and two null states when either the three top or bottom switching devices are turned on. From Tables I and II, the switching modes of the VSC is to be mapped into those of the CSC. After manipulation of these Tables using Karnaugh mapping technique, the two switching modes are related as :

$$\begin{aligned} &T_{ap} = S_{cn}S_{ap} + S_{bn}S_{bp},\ T_{bp} = S_{bp}S_{an} + S_{cn}S_{cp},\\ &T_{cp} = S_{cp}S_{bn} + S_{an}S_{ap},\ T_{cn} = S_{cn}S_{bp} + S_{an}S_{ap},\\ &T_{an} = S_{cp}S_{an} + S_{bn}S_{bp},\ T_{bn} = S_{bn}S_{ap} + S_{cn}S_{cp} \end{aligned} \qquad (3)$$

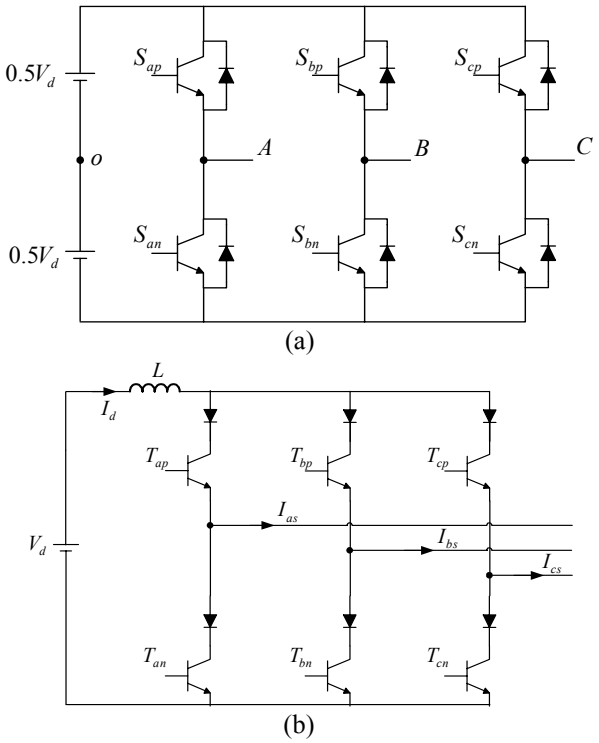

Figure 1. (a) Three-phase voltage source converter, (b) three-phase current source converter

From (3), only one device in the top and bottom are turned ON at any given time. However, according to conditions given by (2), the null states of the VSC cannot be mapped into that of the CSC because the output of this product term will always be zero. The algorithm of (3) on its own can be used for generating the gating signals for a CSC but it won't allow the utilization of the available three null states S_{ap} S_{an}, S_{bp} S_{bn}, and S_{cp} S_{cn} which are required for freewheeling. The required freewheeling can be achieved by connecting another switching device after the input inductor; increasing the count of the switching devices [9-10]. However, the freewheeling can be done without adding an extra switching device by using the null states. Thus, additional conditions- minimization of the number of switch transitions, balancing switch utilization, symmetry in the output switched currents in order to have minimum harmonic distortion and reduction of losses can be imposed. To satisfy the above requirements a logic circuit is developed to detect the condition when the null state in (3) has

to be applied. Once the condition for null state is detected, one of the three legs of the CSC has to be shorted. This is done by gating the devices in the same leg by a common signal, which will be termed as a *shorting pulse*. The optimized sequence of leg shorting is achieved using the absolute maximum of the line-line of the reference modulation signals so that when 'line-line' current I_{ab} is maximum, leg 'a' is shorted, if I_{bc} is maximum leg 'b' is shorted , and when I_{ca} is maximum we short leg 'c'. This algorithm is proven by computer simulation to achieve minimum switching transition, switching symmetry and balanced switch utilization.

TABLE I. SWITCHING STATES FOR CSC

	State	T_{ap}	T_{an}	T_{bp}	T_{bn}	T_{cp}	T_{cn}
ACTIVE	T_1	1	0	0	0	0	1
	T_2	0	0	1	0	0	1
	T_3	0	1	1	0	0	0
	T_4	0	1	0	0	1	0
	T_5	0	0	0	1	1	0
	T_6	1	0	0	1	0	0
NULL	T_7	1	1	0	0	0	0
	T_8	0	0	0	0	1	1
	T_9	0	0	1	1	0	0

TABLE II. SWITCHING STATES FOR VSC

State	S_{ap}	S_{bp}	S_{cp}	S_{an}	S_{bn}	S_{cn}	On Switches
Null, S_0	0	0	0	1	1	1	$T_{an}T_{bn}T_{cn}$
S_1	0	0	1	1	1	0	$T_{cp}T_{an}T_{bn}$
S_2	0	1	0	1	0	1	$T_{bp}T_{an}T_{cn}$
S_3	0	1	1	1	0	0	$T_{bp}T_{cp}T_{an}$
S_4	1	0	0	0	1	1	$T_{ap}T_{bn}T_{cn}$
S_5	1	0	1	0	1	0	$T_{ap}T_{cp}T_{bn}$
S_6	1	1	0	0	0	1	$T_{ap}T_{bp}T_{cn}$
Null, S_7	1	1	1	0	0	0	$T_{ap}T_{bp}T_{cp}$

A. Layout and gating pattern signals

The gating pulse generated using the GDPWM for three phase voltage source converters (S_{ap}… S_{cn}) are obtained by comparing the modulation signals (M_{ip}) [given in (4) for the three top devices] with a high frequency carrier triangular signals. The expressions for the modulation signals are adopted from that of the VSC in which the voltage quantities in the original expressions have been replaced with currents and the phase shift between VSC and CSC space vector accounted for. In (4), ω is the angular frequency of the reference current and δ is the modulation phase angle, I_{is} (I_{as}, I_{bs}, I_{cs}) are the reference phase currents. These generalized discontinuous carrier-based modulation signals clamp the devices for some period of the fundamental frequency to either the positive or negative rail in the process of which the modulator performance may be improved. By varying the modulation phase angle δ, various types of carrier-based generalized discontinuous PWM modulation signals [GDPWM] are obtained [12-14] .

$$M_{ip} = 2\, I_{ip}/ I_d + (1-2\,\sigma) - 2\,\sigma\, I_{max}/ I_d + 2\, I_{min}\,(\sigma -1)/ I_d ,$$

$$\xi\, I_{ap} = I_{as} - I_{bs},\ \xi\, I_{bp} = I_{bs} - I_{cs},\ \xi\, I_{cp} = I_{cs} - I_{as} ,\ \xi = \sqrt{3}$$

$$I_{max} = \mathrm{Max}\,(I_{ap}, I_{bp}, I_{cp}) ,\ I_{min} = \mathrm{Min}\,(I_{ap}, I_{bp}, I_{cp})$$

$$\sigma = 0.5[1 + \mathrm{Sgn}(\mathrm{Cos}\ 3(\omega t + \delta))] ,\ i = a,b,c \qquad (4)$$

The pulses obtained from this modulation scheme are entered into (3) to obtain corresponding pulses for the CSC. Then when the null states are detected, the shorting logic described above and shown schematically in Figure 2 is implemented to short a leg of the CSC.

III. DISCONTINUOUS PWM MODULATION

In this section the direct generalized discontinuous modulation signals for the six switching devices of the current source converter are determined using the classical space vector approach . The qd stationary reference frame currents for all the feasible active and null states are graphically shown in Figure 3 given that the input current is I_d. A reference three-phase current expressed in the stationary reference frame I_{qd}^* located in a sector in Figure 3 is synthesized by time-averaging the two adjacent non-zero state and one of the three null states :

$$\mathbf{I_{qd}^*} = I_{qda}\, t_a + I_{qdb}\, t_b + I_{qd7}\, t_7 + I_{qd8}\, t_8 + I_{qd9}\, t_9 \qquad (5)$$

$$t_a + t_b + t_7 + t_8 + t_9 = 1,\ t_7 = \alpha\,(1- t_a - t_b),\ t_8 = \beta\,(1- t_a - t_b)$$

$$t_9 = \gamma\,(1- t_a - t_b),\ \ \alpha + \beta + \gamma = 1,\ \ \alpha\,\beta = 0,\ \alpha\,\gamma = 0,\ \beta\,\gamma = 0$$

The normalized times t_a, t_b, t_7, t_8, t_9 are respectively the turn-on times of the devices constituting the adjacent states bordering the current reference and the three null states while α, β, γ are the weighting factors for which the null states are used. The equations for the times t_a and t_b from (5) are expressed in terms of the phase reference currents in Table III.

Figure 4 shows the switching functions (unit magnitude) of the switching devices when operating in sector I expressed in terms of the normalized times. The expression for the modulation signal required to generate the PWM pulses to turn on each device is the sum of the times the respective devices are turned on. The expressions of the total turn-on times of each device (τ_{ij}) and the corresponding modulation signals (M_{ij} , i = a,b,c, j = p, n) expressed in terms of the reference three-phase currents (I_{as}, I_{bs} , I_{cs}) using Table III, are given in Table IV. It is the basis for the implementation of the generalized direct digital space vector PWM modulation

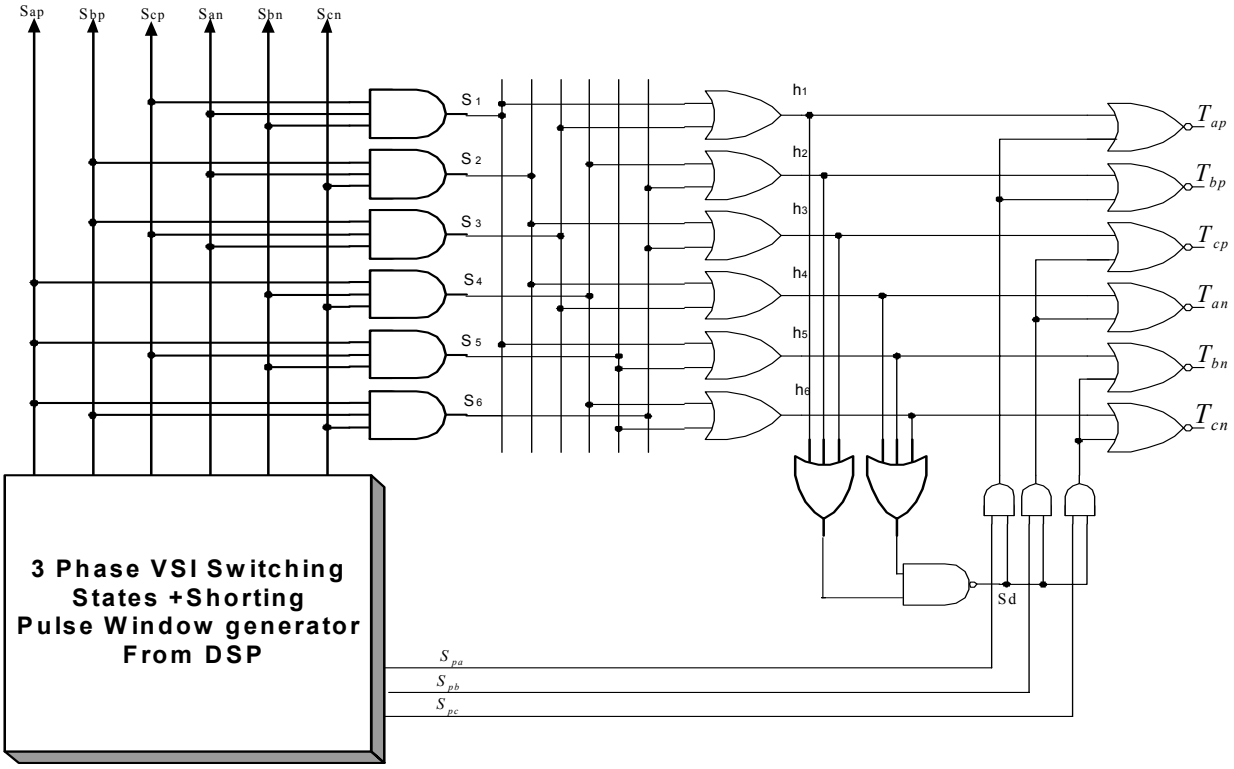

Figure 2. Generation of current source GDPWM modulation signals from voltage source converter modulation

TABLE IV. GENERALIZED DISCONTINUOUS MODULATION SIGNALS (M_{ij}) AND TOTAL TURN-ON TIMES (τ_{ij}) FOR THE CSC

Sector	M_{ap} (τ_{ap})	M_{an} (τ_{an})	M_{bp} (τ_{bp})	M_{bn} (τ_{bn})	M_{cp} (τ_{cp})	M_{cn} (τ_{cn})
I	$I_{as} + \alpha (1+ I_{bs})$ $t_a + \alpha t_c$	$\alpha (1+ I_{bs})$ αt_c	$\beta (1+ I_{bs})$ βt_c	$-I_{bs} + \beta (1+ I_{bs})$ $t_a + t_b + \beta t_c$	$I_{cs} + \gamma (1+ I_{bs})$ $t_b + \gamma t_c$	$\gamma (1+ I_{bs})$ γt_c
II	$\alpha (1- I_{cs})$ αt_c	$-I_{as} + \alpha (1-I_{cs})$ $t_b + \alpha t_c$	$\beta (1- I_{cs})$ βt_c	$-I_{bs} + \beta (1- I_{cs})$ $t_a + \beta t_c$	$I_{cs} + \gamma (1- I_{cs})$ $t_a + t_b + \gamma t_c$	$\gamma (1- I_{cs})$ γt_c
III	$\alpha (1+ I_{as})$ αt_c	$-I_{as} + \alpha (1+ I_{as})$ $t_a + t_b + \alpha t_c$	$I_{bs} + \beta(1+ I_{as})$ $t_b + \beta t_c$	$\beta (1+ I_{as})$ βt_c	$I_{cs} + \gamma (1+ I_{as})$ $t_a + \gamma t_c$	$\gamma (1+ I_{as})$ γt_c
IV	$\alpha (1- I_{bs})$ αt_c	$-I_{as} + \alpha (1-I_{bs})$ $t_a + \alpha t_c$	$I_{bs} + \beta (1- I_{bs})$ $t_a + t_b + \beta t_c$	$\beta (1- I_{bs})$ βt_c	$\gamma (1- I_{bs})$ γt_c	$-I_{cs} + \gamma (1- I_{bs})$ $t_b + \gamma t_c$
V	$I_{as} + \alpha (1+ I_{cs})$ $t_b + \alpha t_c$	$\alpha (1+ I_{cs})$ αt_c	$I_{bs} + \beta (1+ I_{cs})$ $t_a + \beta t_c$	$\beta (1+ I_{cs})$ βt_c	$\gamma (1+ I_{cs})$ γt_c	$-I_{cs} + \gamma (1+I_{cs})$ $t_a + t_b + \gamma t_c$
VI	$I_{as} + \alpha (1- I_{as})$ $t_a + t_b + \alpha t_c$	$\alpha (1- I_{as})$ αt_c	$\beta (1- I_{as})$ βt_c	$-I_{bs} + \beta (1- I_{as})$ $t_b + \beta t_c$	$\gamma (1- I_{as})$ γt_c	$-I_{cs} + \gamma (1- I_{as})$ $t_a + \gamma t_c$

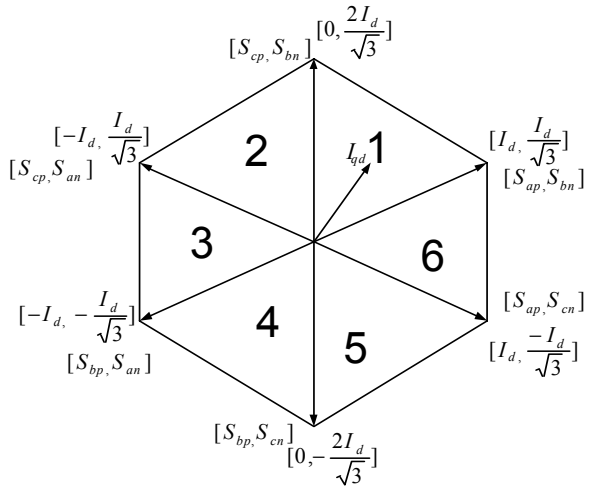

Figure 3. Stationary reference frame space vector current in CSC

TABLE III. EXPRESSIONS FOR TIME t_a AND t_b

Time	Sector I	Sector II	Sector III	Sector IV	Sector V	Sector VI
t_a I_d	I_{as}	$-I_{bs}$	I_{cs}	$-I_{as}$	I_{bs}	$-I_{cs}$
t_b I_d	I_{cs}	$-I_{as}$	I_{bs}	$-I_{cs}$	I_{as}	$-I_{bs}$

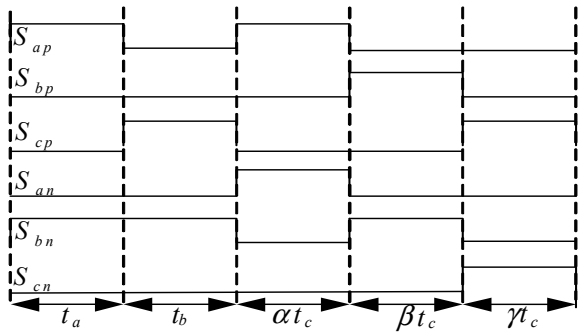

Figure 4. Existence function for the three-phase current source converter operating in sector I .

schemes which are realizable by various selections of the null state variables α, β γ. The DSP/FPGA realization of this scheme is beyond the scope of this paper. It turns out that the linearizing pulse-width modulation (LPWM) realized in hardware in [11] is one of the possibilities in Table IV when $\alpha = 1$ in sectors 3, 6, $\beta = 1$ in sectors 2, 5 and $\gamma = 1$ in sectors 1,4 .

The generalized discontinuous modulation signal expressions shown in Table IV are used for the triangle intersection implementation in which they are compared with a high frequency triangle to generate the switching pulses for the six devices. Unfortunately, if the comparison is done as it is usual especially for VSC, the constraint equations in (1) will be violated. Hence, another method for the switching pulse generation is utilized in this work. The phases with the instantaneous maximum, minimum and medium values of the reference three-phase currents are identified. For the top devices, the modulation signal in Table IV of the phase for which one of the reference currents has a maximum value (M_{ip} where i is the phase with the maximum instantaneous value of the reference currents) is compared with the high frequency triangle to give $S_{ip} = 1.0$ if the modulation signal is greater than the triangle. Otherwise, the top device connected to the phase which has the instantaneous medium value of the three-phase reference currents is turned on. In the case of the bottom device, the modulation signal (M_{in}) of the phase for which one of the reference currents is minimum is compared to the triangle and $S_{in} = 1.0$ if the modulation signal is greater than the triangle. Otherwise, the bottom device connected to the phase for which one of the reference currents is the medium value is turned on.

IV. CONTINUOUS PWM MODULATION

For completeness, the expressions for the modulation signals required for continuous PWM are also derived. The defining equations for the CSC from Figure 1(b) are given as :

$$I_{as} = I_d (T_{ap} - T_{an}) , I_{bs} = I_d (T_{bp} - T_{bn})$$
$$I_{cs} = I_d (T_{cp} - T_{cn}) , \; T_{ij} = 0.5 (2/3 + M_{ij}) \quad (6)$$

Equations (1) and (6) which are under-determined are solved to determine the expressions for the six unknown modulation signals (M_{ij}). There is an infinite number of solutions which are obtained by various optimizing performance functions defined in terms of the modulation signals. For a set of linear indeterminate equations expressed as AX =Y, a solution which minimizes the sum of squares of the variable X is obtained using the Moore-Penrose inverse [15]. The solution given as $X = A^T[AA^T]^{-1}Y$ is for the minimization of the sum of the squares of the six modulation signal .

$$M_{ip} = - M_{in} = 0.5 I_{is}/ I_d , \; i = a,b,c \quad (7)$$

The algorithm described in Section 3 for the synthesis of the switching pulses using the generalized discontinuous carrier-based triangle intersection PWM also applies for the continuous PWM.

V. EXPERIMENTAL RESULTS

The generalized discontinuous triangle intersection PWM modulation schemes set forth in the proceeding sections were implemented with a TMS 320LF2407 DSP and used for the synthesis of waveforms for a current source inverter feeding a passive load. The three-phase capacitors shunted across the load has a per-phase value of 60μF. Figure 5 give experimental waveforms for the inverter operating in the linear and over-modulation regions. It is evident in these waveforms that the continuous modulation scheme gives a load voltage waveform with the highest purity while the generalized discontinuous modulation schemes make the

(a)

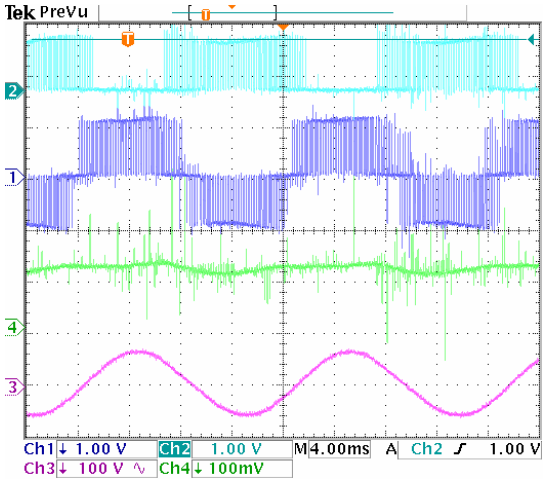

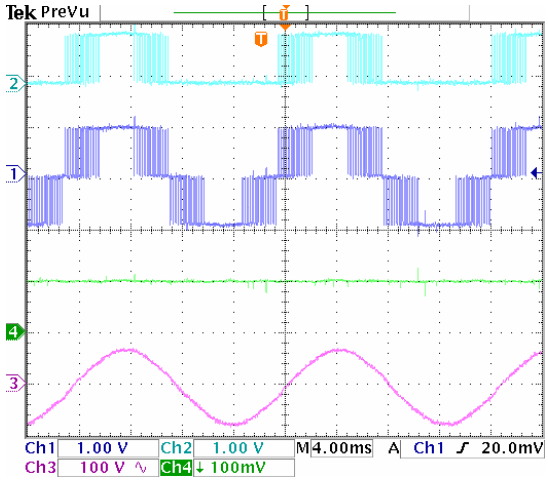

(b)

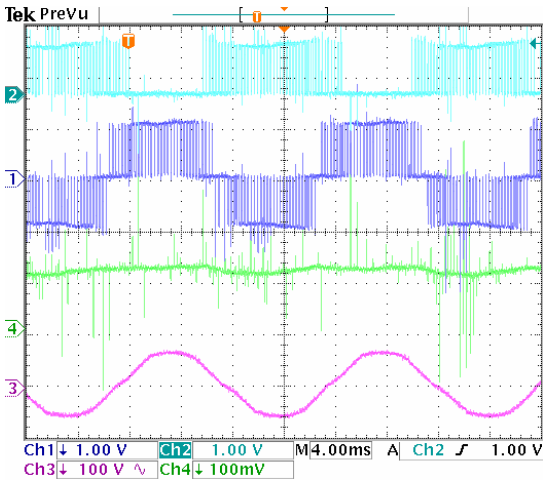

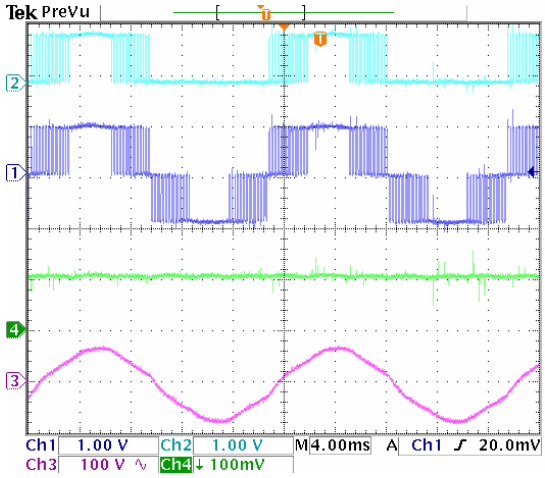

(c)

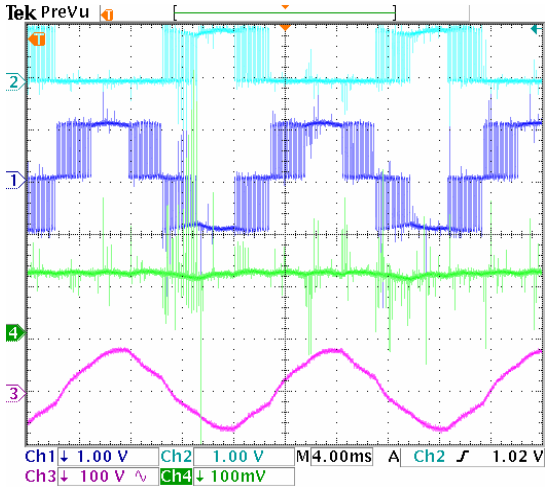

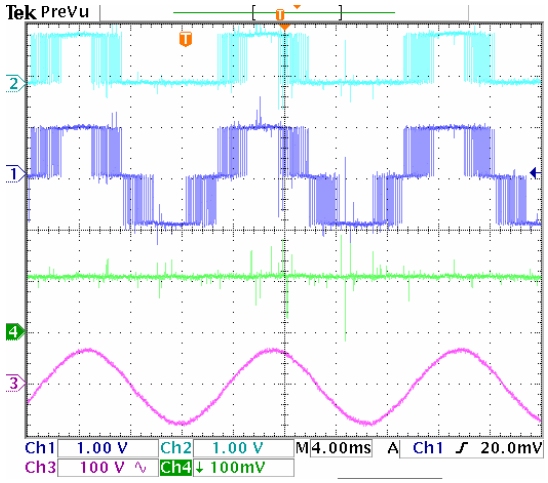

Modulation magnitude index = 0.85

Modulation magnitude index = 1.2

Figure 5: Experimental results for generalized discontinuous PWM modulation. Input dc current = 3 A. From top : (1) device 'a' switching function, (2) phase 'a' current flowing into the load, (3) input dc current, (4) phase 'a' load voltage. (a) Continuous modulation signals , (b) $\alpha = 1$ in sectors 3 and 6, $\beta = 1$ in sectors 2 and 5, $\gamma = 1$ in sectors 1 and 4 , (c) $\alpha = 1$ in sectors 3 and 6, $\beta = 1$ in sectors 2 and 5, $\gamma = 1$ in sectors 1 and 4.

(a)

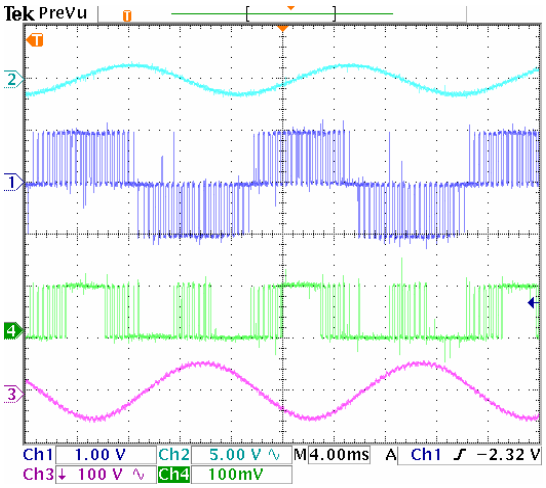

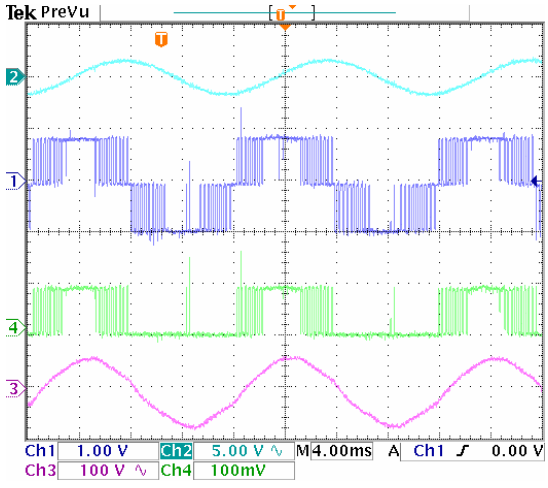

(b)

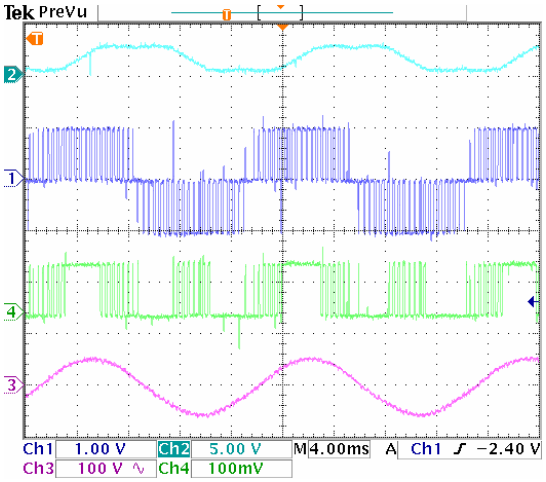

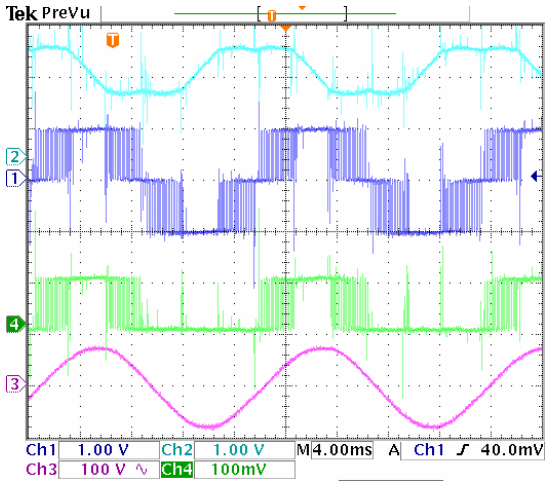

(c)

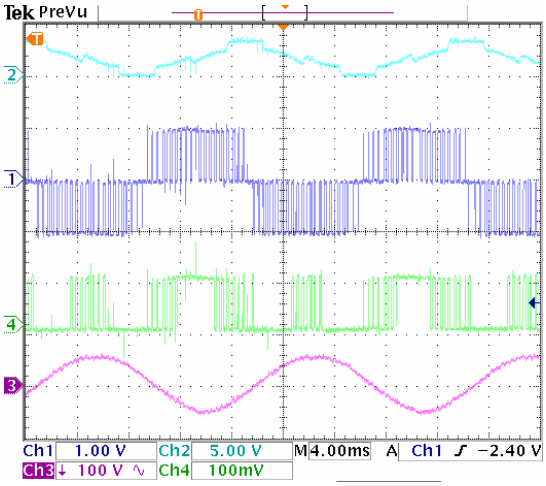

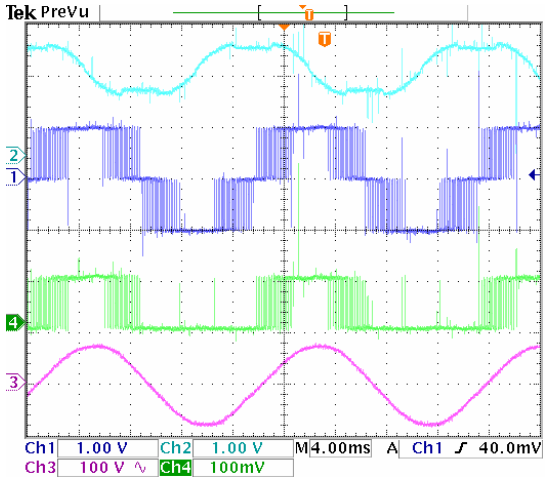

Modulation magnitude index = 0.85

Modulation magnitude index = 1.2.

Figure 6: Experimental results using voltage source converter generalized discontinuous PWM modulation. Input dc current = 3 A. From top : (1) top device ‘a’ modulation signal, (2) phase ‘a’ current flowing into the load, (3) top device ‘a’ switching function, (4) phase ‘a’ load voltage. (a) Continuous modulation signals, (b) classical space vector $\sigma = 0.5$, (c) modulation control angle $\delta = 0.0^{o}$.

switching devices to switch less, ensuring lower switching loss and effective switching frequency. In figure 6, waveforms for the inverter using the generalized discontinuous modulation for voltage source converters are shown. Comparatively, the waveforms of Figure 6 are better than those of Figure 5 where the direct generalized discontinuous modulation scheme is used. Thus the only difference would lie in the amount of device switching loss and the output waveform quality. It is observed from experimental results (not shown in this paper) that space vector PWM with $\sigma = 0.5$ has more switching transitions than its discontinuous counterparts to generate the same output voltages.

VI. CONCLUDING REMARKS

This paper presents two different schemes for the modulation of the three-phase current source converters. The direct generalized discontinuous modulation scheme is obtained using an approach similar to the classical space vector and can be implemented either by direct digital space vector implementation or as a carrier-based triangle intersection methods. Also, starting from the equations for the generalized discontinuous modulation signals for the three-phase voltage source converter, the corresponding modulation method for the current source converters was determined and generalizes some of the implementations reported in [16-17]. The triangle intersection versions of the modulation techniques have been experimentally implemented and converter waveforms shown in Figures 5 -8, confirm the efficacy of the schemes. The known advantages of discontinuous modulation schemes in voltage source converters – reduced switching loss, reduced effective switching frequency, extended linear region during over-modulation are carried over to the three-phase current source converters. Hence the proposed generalized discontinuous modulation schemes should find utility in applications where loss minimization is desired. It would appear that for the modulation scheme given in Section 3, the discontinuous modulation scheme can be used in the over-modulation region and complemented with the continuous modulation when the converter operates in the linear region. In similar fashion, the method set forth in Section 2, it will be useful to use the modulation signals for the classical space vector when operating in the linear modulation region and transit to the discontinuous modulation scheme (selecting appropriate δ that meets a required performance objective) when operation in the over-modulation region is required.

REFERENCES

[1] J. R. Espinoza and G. Joos, "Current source converter on-line pattern generator switching frequency minimization," IEEE Trans. on Industrial Electronics, vol. 44, no. 2, pp. 198-206, April 1997.

[2] C. Namuduri and P. Sen, "Optimal pulse-width modulation for current source inverters," IEEE Trans. on Industry Applications, vol. 22, no. 6, pp. 1052 – 1072, November/December 1986.

[3] H. Karshenas, H. Kojori and S. Dewan, "Generalized techniques of selective harmonic elimination and current control in current source inverter/converters," IEEE Trans. on Power Electronics, vol. 10, no. 5, pp. 566 – 573, September 1995.

[4] J. R. Espinoza, G. Joos, "State variable decoupling and power flow control in PWM current source rectifiers," IEEE Trans. on Industrial Electronics, vol. 45, no. 1, pp. 78 – 87, February 1998.

[5] G. Ledwich, "Current source inverter modulation," IEEE Trans on Power Electronics, vol. 6, pp. 618-623, July 1991.

[6] D. N. Zmood and D. G. Holmes, "A generalized approach to the modulation of current source inverters," Conference Record of the IEEE Power Electronics Society Specialist Conference, pp. 739 – 746, June 1998.

[7] D. N. Zmood and D. G. Holmes, "Improved voltage regulation for current source inverters," IEEE Trans. on Industry Applications, vol. 37, no. 4, pp. 1028 – 1036, July/August 2001.

[8] D. G. Holmes and T. A. Lipo, Pulse-width Modulation for Power Converters, IEEE Press, New York, 2003.

[9] I. Wallace, A. Bendre, J. P. Nord, G. Venkataramanan, " A unity power factor three-phase PWM SCR rectifier for high power applications in the metal industry," IEEE Trans. on Industry Applications, vol. 38, no. 4, pp. 898-908, July/August 2002.

[10] A. Bendre, I. Wallace, J. Nord and G. Venkataramanan, " A current source PWM inverter with actively commutated SCRs," IEEE Trans. on Power Electronics, vol. 17, no. 4, pp. 461 – 268, July 2002.

[11] K. D. T. Ngo and Jun Chen, "Integrator – based linearizing pulse-width modulator for three-phase inverters," IEEE Trans. on Power Electronics, vol. 18, no. 2, pp. 612- 618, March 2003.

[12] Vladimir Blasko, "Analysis of a Hybrid PWM Based on Modified Space Vector and Triangle Comparison Methods," IEEE Trans. on Industry Applications, Vol. 33, No. 3, pp. 756-764, May/June 1997.

[13] O. Ojo "The generalized discontinuous PWM modulation scheme for three-phase voltage source inverters," To appear in the IEEE Trans. on Industrial Electronics, October 2004.

[14] A. Hava, R. J. Kerkman and T. A. Lipo, "A High Performance Generalized Discontinuous PWM Algorthim," IEEE Trans. on Industry Applications, vol. 34, no. 5, pp. 1059-1071, September/October 1998

[15] R. Stengel, Stochastic **Optimal Control**, John Wiley, New York, 1986.

[16] J. R. Espinoza, G. Joos, J. Guzman, L. Moran, R. Burgos, "Selective harmonic elimination and current/voltage control in current/voltage source topologies : A unified approach," IEEE Trans. on Industrial Electronics, vol. 48, no. 1, pp. 71 – 81, February 2001.

[17] V. Agelidis, P. Ziogas and G. Joos, "Dead-band PWM switching patterns," Conference record of the IEEE-Power Electronics Specialists Conference, pp. 427 – 434, 1992.